EARTH SURFACE PROCESSES AND LANDFORMS
Earth Surf. Process. Landforms **36**, 1218–1229 (2011)

Published online 18 March 2011 in Wiley Online Library
(wileyonlinelibrary.com) DOI: 10.1002/esp.2147

Modelling wind-blown sediment transport around single vegetation elements

Jakolien K. Leenders,[1,2] Geert Sterk[3]* and John H. Van Boxel[4]
[1] HKV Consultants, Lelystad, The Netherlands
[2] Land Degradation and Development group, Wageningen University, Wageningen, The Netherlands
[3] Department of Physical Geography, Faculty of Geosciences, University of Utrecht, Utrecht, The Netherlands
[4] Institute for Biodiversity and Ecosystem Dynamics (IBED), University of Amsterdam, Amsterdam, The Netherlands

Received 28 May 2010; Revised 7 February 2011; Accepted 7 February 2011

* Correspondence to: Geert Sterk, Department of Physical Geography, Faculty of Geosciences, University of Utrecht, Utrecht, The Netherlands. E-mail: g.sterk@geo.uu.nl

ESPL
Earth Surface Processes and Landforms

ABSTRACT: Wind erosion is an important soil erosion and hence a soil degradation problem in the Sahelian zone of West Africa. Potentially, the characteristic dryland vegetation with scattered trees and shrubs can provide for soil erosion protection from wind erosion, but so far adequate quantification of vegetation impacts is lacking. The aim of this study was to develop a model of wind-blown soil erosion and sediment transport around a single shrub-type vegetation element. Starting with the selection of a suitable transport equation from four possible sediment transport equations, the effects of a single vegetation element on wind speed were parameterized. The modified wind speed was then applied to a sediment transport equation to model the change in sediment mass flux around a shrub. The model was tested with field data on wind speed and sediment transport measured around isolated shrubs in a farmer's field in the north of Burkina Faso. The simple empirical equation of Radok (*Journal of Glaciology* **19**: 123–129, 1977) performed best in modelling soil erosion and sediment transport, both for the entire event duration and for each minute within an event. Universal values for the empirical constants in the sediment transport equation could not be obtained because of the large variability in soil and roughness characteristics. The pattern of wind speed, soil erosion and sediment transport behind a shrub and on either side of it was modelled. The wind speed changed in the lee of the vegetation element depending on its porosity, height and downwind position. Wind speed was recovered to the upstream speed at a downwind distance of 7·5 times the height of the shrub. The variability in wind direction created a 'rotating' area of influence around the shrub. Compared to field measurements the model predicted an 8% larger reduction in sediment transport in the lee of the vegetation element, and a 22% larger increase beside the vegetation element. Copyright © 2011 John Wiley & Sons, Ltd.

KEYWORDS: Sahel; wind erosion; scattered vegetation; wind speed pattern; sediment transport; modelling

Introduction

Wind-blown sediment transport is a widespread phenomenon in the Sahelian zone of Africa, which has many adverse effects. Severe soil degradation can occur as a result of the loss of relatively fertile top soil material (Sterk *et al.*, 1996; Sterk, 2003). Crop damage by abrasion or burial by sand during storms can also occur (Sterk and Haigis, 1998). In addition, it can give rise to health problems due to the occurrence of large amounts of dust in the air (Alfaro *et al.*, 2004) and it can result in sedimentation at undesired places (Mohammed *et al.*, 1995).

Sediment can be entrained whenever the force of the wind exceeds the resistance of the soil particles. When sediment is entrained, the material can be transported in three transport modes: creep, saltation and suspension (Bagnold, 1941). The very fine to coarse sand fraction of the sediment (approximately 70–1000 μm) is mainly transported in saltation, the bouncing motion of grains. Saltation also initiates the other two transport modes: creep, the rolling and sliding of large particles (>1000 μm) over the surface, and suspension, the raising of fine soil particles (<70 μm) in the air (Shao, 2000). As wind direction, wind speed and duration of wind erosion events is variable, the amount of sediment transported in each event is also variable.

The variability of sediment transport is further enhanced by the erodibility of a soil, which also varies in space and time. Erodibility is determined by several variables such as: soil moisture (Chepil, 1956; Namikas and Sherman, 1995), soil texture (Fryrear *et al.*, 1994), presence of surface crusts (Rice and McEwan, 2001; Goossens, 2004), soil cover (Fryrear, 1985), surface roughness (McKenna Neuman, 1998) and topography (Iversen and Rasmussen, 1999; Sterk *et al.*, 2004). These variables might limit the entrainment of particles in the air and cause sediment transport to be supply-limited. In addition, some of these variables (e.g. soil coverage and surface roughness) might induce trapping of sediment once it is entrained and being transported (Raupach *et al.*, 2001).

Given the many adverse effects of Sahelian wind erosion (Sterk, 2003), there is a need to develop measures or strategies to prevent wind erosion. Studies of farmers' perceptions in Niger and Burkina Faso (Taylor-Powell, 1991; Rinaudo, 1996; Sterk and Haigis, 1998; Bielders *et al.*, 2001; Leenders *et al.*, 2005b) indicated that scattered woody vegetation (trees and shrubs) potentially reduces wind erosion in the Sahel. This was supported by a study on the pattern of sediment transport around a single vegetation element (Leenders *et al.*, 2007). Scattered vegetation reduces sediment transport in three ways (Van de Ven *et al.*, 1989; Wolfe and Nickling, 1993): (1) it shelters the soil from the erosive force of the wind by covering a proportion of the surface; (2) it reduces the wind velocity by extracting momentum from the flow; (3) it traps sediment particles.

In the past, the influence of scattered vegetation elements on the wind force has been quantified using the shear stress partitioning theory. This theory is based on the classical work by Schlichting (1936) and Marshall (1971), who both studied the aerodynamics of rough surfaces using a variety of roughness elements. In the shear stress partitioning theory, the total shear stress, expressed by the friction velocity (u_*), is partitioned into a part that is absorbed by the roughness elements, and a part that acts on the bare surface between the elements. In several studies the shear stress partitioning theory was tested in the field with real vegetation elements in dry desert-like environments (e.g. Musick and Gillette, 1990; Stockton and Gillette, 1990; Wolfe and Nickling, 1996). In those studies, it was evaluated how the threshold shear velocity, expressed by u_{*t}, for sediment transport changed due to the number, shape and surface cover of vegetation elements. More recently, Okin (2008) developed a new model of wind erosion in the presence of vegetation. The model is also based on the shear stress partitioning theory, but uses an alternative approach. It uses the size distribution of erodible gaps between vegetation elements to calculate the shear stress reduction due to vegetation cover. No specific distribution of the vegetation is assumed in the model, instead a probability distribution of the size of unvegetated gaps between the vegetation is used. The model was applied to several data sets from literature and proved to accurately predict shear stress ratios for different vegetation covers.

Despite the quantitative knowledge about the influence of scattered vegetation elements on wind speed, shear stress and threshold shear velocity, there is generally a lack of quantitative information about the role of such vegetation on aeolian sediment transport. In a previous study, data of wind speed and sediment transport around isolated obstacles were collected in the Sahelian zone of Burkina Faso (Leenders *et al.*, 2007). The next step is to develop appropriate models for prediction of the impacts of scattered vegetation on wind speed and sediment transport. The modelling of wind-blown sediment transport around a single vegetation element is an important step towards exploiting and developing strategies of using scattered vegetation to control soil loss.

The key in modelling sediment transport is to develop the correct parameterization of the driving forces of the wind and the erodibility of the soil. Shear stress is used in most sediment transport equations (Greely and Iversen, 1985). Values of the friction velocity are usually obtained from wind speed profiles averaged over periods of at least 10 minutes (Namikas *et al.*, 2003). This way, friction velocity can be obtained by fitting a logarithmic wind profile to the data. But, behind an obstacle, wakes generated by roughness elements complicate the flow and the velocity profile departs from the logarithmic wind profile (Raupach *et al.*, 1980). The shear stress partitioning theory can be applied to determine the average shear stress on the bare surface area between vegetation elements, but not to model the impact of a single vegetation element on the surrounding wind speed and sediment transport. In addition, the process of sediment transport is highly intermittent and characterized by short periods of intense transport and other periods of no or less intense transport. This intermittency is only noticeable at small timescales (part of a second) (Leenders *et al.*, 2005a). It is therefore questionable whether time-averaged, profile-derived estimates of friction velocity are adequate to characterize the wind field for the purpose of sediment transport modelling at small spatial and temporal scales. When wind speed is measured at a relatively high frequency (>1 Hz), sediment transport correlates well with horizontal wind speed (Sterk *et al.*, 1998; Schönfeldt and Von Löwis, 2003; Leenders *et al.*, 2005a).

The central issue in modelling sediment transport is to estimate the amount of sediment transported by the wind. At present, however, there is no model that is uniformly valid at a variety of sites (Dong *et al.*, 2003). This is mainly attributed to the deviation of the ideal conditions in wind tunnels, where most transport models were developed, from the field, where ideal conditions usually are absent (Sherman *et al.*, 1998). The ideal conditions related to the wind forces include a unidirectional, fully turbulent, uniform and steady wind and a wind velocity profile that obeys the logarithmic wind profile when sediment is transported. Ideal conditions related to the erodibility of the soil comprise clean, dry and uniformly-sized sands and a planar and unobstructed surface (Dong *et al.*, 2003). At the spatial scale of a Sahelian farmer's field, these ideal conditions are not met, amongst others due to the presence of a variety of (isolated) vegetation elements.

The ultimate goal is to develop a model that enables prediction of sediment transport in an entire Sahelian field with scattered vegetation. To reach this goal, first an appropriate model for the sediment transport around a single vegetation element should be developed. The aim of this paper, therefore, was to develop a model of wind-blown sediment transport around a single vegetation element. Specific objectives were: (1) to evaluate transport equations for adequate predictions of sediment transport; (2) to parameterize the effects of a single vegetation element on wind speed and sediment transport in two dimensions.

Model Concept

Two-dimensional modelling of sediment transport around a single vegetation element involves two parameterizations: (1) spatial representation of the areas around a vegetation element in which sediment transport is affected, and (2) quantification of sediment transport within the affected areas. Modelling was done by calculating wind speed around a single vegetation element, then applying a quantitative sediment transport equation to determine the distribution of horizontal mass flux in the vicinity of the vegetation element. The model performs these calculations several times during the course of a wind erosion event and is therefore a dynamic model. This was done to capture the variability in wind speed and wind direction during a storm event. The model was especially developed for shrubs, defined as vegetation elements with a canopy starting at the soil surface.

Spatial representation

The area around a shrub in which sediment transport is affected involves a zone of reduction in sediment transport

downwind of the shrub, and a zone of increase in sediment transport at the sides. Such patterns of wind speed changes have been experimentally quantified by Ash and Wasson (1983) and Leenders *et al.* (2007). The shrub was placed in a grid with a spacing of 0·1 m to make the model spatially explicit. The zones of reduction and increase around the shrub were described by different ellipses, of which the major axes are oriented in the direction of the wind. An ellipse centred at the origin of an *x*–*y* coordinate system with its major axis along the *x*-axis is defined by the equation:

$$\left(\frac{x}{a}\right)^2 + \left(\frac{y}{b}\right)^2 = 1 \quad (1)$$

in which *a* equals the half length of the major axis and *b* equals the half length of the minor axis.

Downwind of a shrub, a zone of reduction in wind speed and sediment transport exists that extends downwind to 7·5 times the height of the vegetation element (Leenders *et al.*, 2007). This reduction zone is modelled with an ellipse in which *a* was set to 7·5 times the height of the vegetation element, and *b* was set to 0·5 times the width of the vegetation element lateral to the wind direction. As such the minor axis of the reduction ellipse was set equal to the width of the vegetation element lateral to the wind direction (Figure 1A). The origin of the ellipse was located at the centre of the vegetation element (0,0). The reduction of wind speed upwind of the shrub was neglected.

Within the reduction zone behind a shrub, sub-ellipses exist that correspond to a factor of reduction in sediment transport. The largest reduction in sediment transport was close behind the obstacle, recovering gradually to the sediment transport of the approach flow. At a distance of 7·5 times the height of the vegetation element, the sediment transport had recovered to the upstream sediment transport (Figure 1B).

To the sides of a shrub, lateral to the wind direction, wind speed was observed to accelerate (Ash and Wasson, 1983; Leenders *et al.*, 2007). The zones of increase in wind speed on both sides of the shrub were also described by an ellipse. For this ellipse, factor *a* was set to 0·5 times the width of the shrub in the direction of the wind (*x*-axis), because the effect of increase in wind speed can be expected to apply over the entire width of the shrub. The factor *b* was set to 0·25 times the width of the shrub lateral to the wind direction. These values were based on measured wind speeds around shrubs by Leenders *et al.* (2007), and are in agreement with the pattern observed by Ash and Wasson (1983). The origins of these ellipses were located at (0, $y \pm 0{\cdot}75$ times the lateral width of the shrub) (Figure 1C).

The shrub itself was also represented by an ellipse, to enable simulation of circular as well as elongated vegetation elements. In the ellipse representing the shrub *a* is half of the width of the vegetation element in an east–west direction ($0{\cdot}5{\cdot}W_{EW}$) and *b* is half of the width of the vegetation element in a north–south direction ($0{\cdot}5{\cdot}W_{NS}$). Because for each time step during an event, the *x*-axis was oriented in the direction of the wind, and thus the width of the vegetation element lateral to the wind direction changed for each time step. This has been taken into account by:

$$W_y = 2\sqrt{\frac{(0.5W_{NS})^2 \cdot (0.5W_{EW})^2}{(0.5W_{NS})^2 \cos^2\alpha + (0.5W_{EW})^2 \sin^2\alpha}} \quad (2)$$

where W_y is the width of the vegetation element lateral to wind flow, $0{\cdot}5W_{EW}$ the half width of the vegetation element in east–west direction, $0{\cdot}5W_{NS}$ the half width of the vegetation element in north–south direction, and α the wind direction.

Quantification of sediment transport

The second parameterization in modelling involved the quantification of sediment transport in the areas affected by the shrub. Quantification of the change in wind speed around the shrub was the first step in quantification of sediment transport. In the area of increase in sediment transport, the average factor of change in wind speed (Φ) was observed to be 1·06 (Leenders *et al.*, 2007). In the ellipses of increase in wind speed at the sides of a shrub, Φ was modelled with a simple parabolic curve. As such, the factor Φ changes from 1·0 at the borders of the increase ellipse to 1·12 at the centre, with an average of 1·06:

$$\Phi = -0.12\left(\left(\frac{x}{0.5W_y}\right)^2 + \left(\frac{y}{0.25W_y}\right)^2\right)^2 + 1.12 \quad (3)$$

where Φ is the factor of change in wind speed; *x* the coordinate of the increase ellipse along the wind direction, *y* the coordinate of the increase ellipse lateral to the wind direction; and W_y the width of the shrub lateral to the wind direction.

In the area of reduction in sediment transport, the factor of change in wind speed along the centre line was described by modifying Hagens' (1996) friction velocity reduction factor (fu_*) behind a windbreak. Although this reduction factor was developed for describing the profile of friction velocity it was assumed here that it can be used for describing wind speed reduction as well. Friction velocity and wind speed are

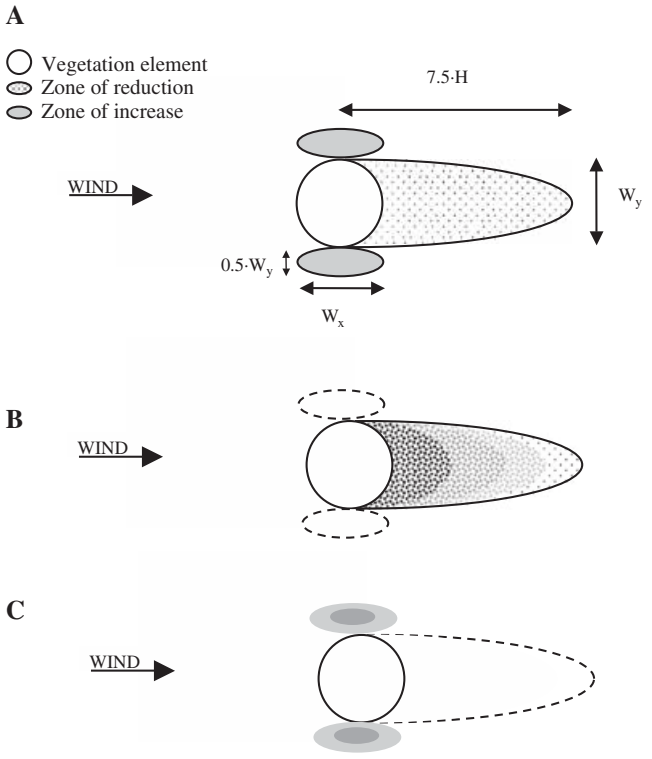

Figure 1. (A) Spatial representation of zones of increase and reduction in total mass flux in the vicinity of a shrub. The dimensions of the zones are a function of the height of the vegetation element (*H*), the width of the vegetation element in the direction of the wind (W_x), and the width of the vegetation element orthogonal to the direction of the wind (W_y). (B) Zone of reduction in wind speed. (C) Zones of increase in wind speed.

linearly related and therefore the pattern of reduction should be similar. The original equation for the reduction factor fu_* is (Hagen, 1996):

$$fu_* = 1 - \exp\left(-c x_H^2\right) + d\exp\left(-0.003(x_H + e)^f\right) \quad (4)$$

where x_H is the distance from the barrier along the wind direction in terms of barrier heights. Coefficients c, d, e and f depend on the barrier porosity (θ) and were expressed by Hagen (1996) as:

$$c = 0.008 - 0.17\theta + 0.17\theta^{1.05} \quad (5)$$

$$d = 1.35\exp(-0.5\ \theta^{0.2}) \quad (6)$$

$$e = 10(1 - 5\theta) \quad (7)$$

$$f = 3 - \theta \quad (8)$$

These variables depend on the porosity of the barrier as the porosity determines the ratio between airflow that passes through the barrier pores and airflow that diverges over the barrier. As such porosity determines the position of minimum wind speed and the rate of recovery of wind speed.

The coefficients c–f (Equations 5–8) were modified to adapt Equation 4 to model the factor of change in wind speed (Φ) along the centre line of the reduction area behind a single shrub. The coefficients c, d, e and f remained to depend on the porosity of the shrub (θ) and x_H was taken as the distance from the shrub centre along the wind direction in terms of shrub height. The four coefficients were fitted to actual measured wind reduction profiles (see Materials and Methods section). At this point we have a factor of change in wind speed at the centre line behind a shrub. By using the general formula of an ellipse a reduction factor of wind speed was assigned to the entire reduction zone behind a shrub (Figure 1B). The reduction zone stretches from the centre of the shrub downwind to 7·5 times the height of the shrub (Leenders *et al.*, 2007).

The thus obtained change in wind speed (Φ) in the reduction zone leeward of the shrub and the increase zones at the sides of the shrub was translated to an adapted wind speed around the shrub. This adapted wind speed was translated to a change in sediment transport with a sediment transport equation. Hence a sediment transport equation had to be selected before the model could be applied (see Materials and Methods section). Since the model simulates wind speed reductions around vegetation elements, we also selected a sediment transport equation based on wind speed instead of friction velocity. Subsequently this sediment transport was normalized with the sediment transport of unobstructed flow to calculate a sediment transport change factor (Ψ). These calculations were done for each time step within the model. Every time step the direction of the x-axis was rotated into the average wind direction for that time step. In this study the time step of the model was set to one minute.

Materials and Methods

Study area

The experimental work for this study was done in 2002 and 2003. The measurements were conducted at a farmer's field near the village Windou, which is located approximately 7 km east of Dori in northern Burkina Faso. The area is part of the southern Sahelian zone of West Africa. Temperatures are high (>15 °C) all year round and the area has a short rainy season of four months from late May to the end of September. The average annual precipitation at Dori is 420 mm.

Wind erosion may occur during two periods, the Harmattan season and the early rainy season. During the Harmattan season (December–March), the dry northeasterly trade winds bring large quantities of dust from the Sahara desert. Much of this dust is deposited in the Sahel and areas further south, but wind erosion in the Sahel itself is of low intensity. In the Sahel severe wind erosion occurs during the early rainy season, when heavy thunderstorms develop that bring the first rains. The strong downdrafts that accompany the thunderstorms and precede rainfall cause intense soil particle movement, especially on bare soils without wind erosion control measures. The events are usually of short duration (10–30 minutes) and are mostly followed by heavy rainstorms (Michels *et al.*, 1995; Sterk, 2003).

The soil in the experimental field has a loamy sand texture, with 85·5% sand, 11·1% silt and 3·4% clay in the topsoil, and a median particle size of 141 μm. The main crop in the field was pearl millet (*Pennisetum glaucum*), intercropped with cowpea (*Vigna unguiculata*). The pearl millet was sown following the first major rain storm in the early rainy season, and the cowpea intercrop was sown approximately four weeks later. The plant density of both crops is low, due to the typical Sahelian cultivation method. Pearl millet is traditionally sown along lines, 1 m apart, in small holes which are also approximately 1 m from each other. The cowpea is sown between the pearl millet lines. In the early stages of the rainy season, when the wind erosion activity is highest, the plant cover is generally low, and only after approximately five to six weeks after sowing the plants are sufficiently large (~0·5 m height) to reduce wind speed and sediment transport. There was also natural vegetation in the field. The density of vegetation elements larger than 0·5 m height was about 70 elements per hectare. Most of these vegetation elements consisted of shrubs (80%). Shrubs are here identified as vegetation elements with branches hanging to the ground. The maximum height of the shrubs was 3·4 m, and the maximum height of trees was 11·0 m. The most common vegetation species were *Piliostigma reticulatum*, *Faidherbia albida*, *Balanites aegyptiaca*, *Sclerocarya birrea* and *Ziziphus mauritiana*.

Equipment

Wind speed was measured using four cup-anemometers (Vector Instruments, Type R30). This anemometer measures wind speeds from 0·2 m s^{-1} up to 55 m s^{-1} with an accuracy of 1%, the distance constant being 2·3 m. This means that during wind erosion events with average wind speeds of 7 to 12 m s^{-1}, the response time of the sensor, defined by the distance constant divided by the wind speed (Camp *et al.*, 1970), is just a fraction of a second (0·2–0·3 seconds). The cup-anemometers were mounted on a mast at heights of 0·75 m, 1·25 m, 2·25 m and 3·25 m and were connected to a CR10 datalogger (Campbell Scientific Ltd). Wind speed was sampled at five-second intervals and the average values were registered every minute.

Sediment transport was measured with two saltiphones placed at 0·10 m above the surface and 17 sediment catchers. A saltiphone is a robust sensor that records saltation transport using a microphone (Spaan and Van den Abeele, 1991). The instrument is able to detect periods and intensities of saltation transport, but cannot be used to quantify the absolute magnitude of particle flux (Goossens *et al.*, 2000). The two saltiphones were placed at a distance of 3 m northeast (NE) and southwest (SW) of the mast with the cup-anemometers (Figure 2). The total counts of saltation transport were stored

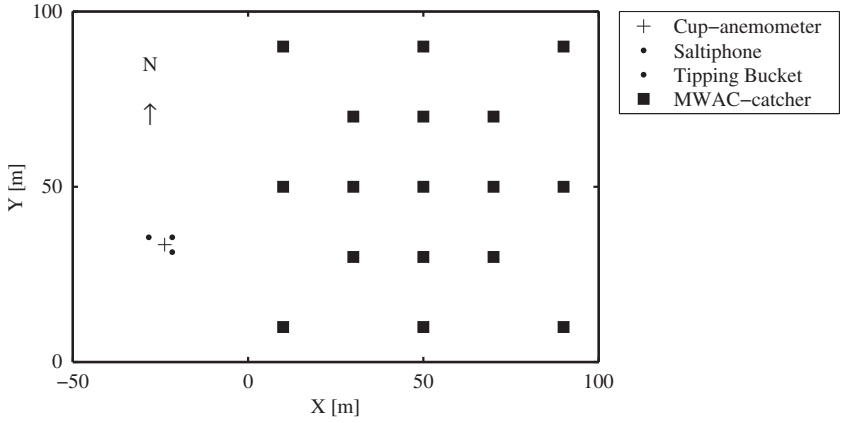

Figure 2. Location of equipment in the experimental field at Windou, north Burkina Faso, during the rainy season of 2003.

in the CR10 datalogger every minute. Data from a tipping bucket rain gauge connected to the same datalogger were used to select the period of sediment transport before rain ensuring that the recorded sediment transport was caused by wind alone.

The aeolian mass flux during a storm was measured with Modified Wilson and Cooke (MWAC) catchers, which trap moving material at different heights. The traps consist of a plastic bottle with an inlet and an outlet glass tube entering the bottle through the cap. The inlet and outlet glass tubes have an internal diameter of 8 mm, which is equivalent to an opening of 50·3 mm^2. Traps are mounted horizontally on a mast and are pointed into the wind by a wind vane connected to the mast. Air and sediment enter through the inlet, sediment settles in the bottle and air escapes through the outlet. The MWAC catchers used in this study measured sediment transport at five heights (0·05, 0·12, 0·19, 0·26 and 0·5 m) above the soil surface, but these values could change up to 20 mm because of soil surface changes during storms. For more details on the MWAC catcher see Sterk and Raats (1996).

During the early rainy seasons of 2002 and 2003 the 17 MWAC catchers were positioned in a regular pattern such that there were always five catchers in a row for the eight cardinal and inter-cardinal wind directions (Figure 2). The aim of those measurements was to obtain median values of the aeolian mass fluxes in the field, which were used here for model development (2003 data) and evaluation (2002 data). An additional set of 17 MWAC catchers was used during the 2002 season to measure sediment transport around single vegetation elements. Those measurements have already been described in Leenders *et al.* (2007), and the data was used in this study to evaluate the developed model. Also the detailed wind speed measurements around single vegetation elements, described in Leenders *et al.* (2007) were used here for model evaluation.

Calculation of transported mass fluxes

Mean horizontal mass flux densities $q(z)$ (in kg m^{-2} s^{-1}) at height z (in metres) were calculated from the event duration and the dry weights of the trapped materials in the MWAC catchers. Subsequently, a mass flux density profile was fitted through the measured mass flux densities to calculate the mass flux. For this purpose, a combined model was used to describe the mass flux densities (Sterk and Raats, 1996). This model was found to be more accurate than a modified power function as suggested by Zingg (1953). The equation of the combined mass flux model is given by:

$$q(z) = k\left(\frac{z}{\beta}+1\right)^{-m} + n\exp\left(-\frac{z}{\gamma}\right) \tag{9}$$

where $q(z)$ is the mass flux density (in kg m^{-2} s^{-1}) at height z (in metres); and k, m and n are regression coefficients. The coefficient m is dimensionless while the coefficients k and n have the dimensions of mass flux density (in kg m^{-2} s^{-1}); the length scales β and γ were taken as 1 m in this study. An extensive description of the model and the fitting method can be found in Sterk and Raats (1996).

The fitted mass flux density profile was integrated over height from 0 to 1 m, to calculate the mass flux Q (in kg m^{-1} s^{-1}) at the sampling location up to 1 m above the soil surface. The total mass flux, Q_t (in kg m^{-1} s^{-1}), was obtained by dividing Q by the trapping efficiency of the catcher. Sterk (1993) obtained an overall trapping efficiency of the MWAC catcher of 0·49 with a standard deviation of 0·03. This was based on 12 runs in a wind tunnel with wind speeds ranging from 9·9 to 11·5 m s^{-1} using comparable soil from the Sahelian zone of Niger. The efficiency remained constant within the range of the tested wind speeds, which was also found by Goossens *et al.* (2000), who tested a single MWAC trap over a much wider wind speed range (6·5–14·5 m s^{-1}). A comparable overall efficiency (0·51) of the MWAC catcher was found by Cornelis *et al.* (2004). Hence, in this study the efficiency of 0·49 was used because we applied the same equation as Sterk (1993) and because the trapping efficiency was determined by using similar Sahelian sand as in our study area.

Fit of transport equations

Four transport equations were used to fit the measured total mass fluxes (Q_t) to wind characteristics (Table I). These were the transport equations of O'Brien and Rindlaub (1936); Kuhlman (1958); Radok (1977); and Dong *et al.* (2003). The model of Radok (1977) is the only fully empirical model in the list, the others have relatively sound theoretical support (Dong *et al.*, 2003). Radok's model (1977) and the model of Kuhlman (1958) have the limitation that they can predict sediment transport even when wind velocity is below threshold. Therefore these models should only be applied for conditions with wind velocities above the threshold wind velocity for sediment transport. For the models of Kuhlman (1958) and Dong *et al.* (2003) this problem is solved by introducing a threshold wind velocity. The threshold wind velocity at both fields was set to 6 m s^{-1} at a height of 3·25 m. This value was determined using the approach of Sterk *et al.* (1999) in which the measured saltiphone counts were plotted against the wind

Table I. Overview of the sediment transport models used in this study (after Dong *et al.*, 2003)

Contributor	Expression	Equation
O'Brien and Rindlaub (1936)	$Q_t = C_1\ (\rho/g)\ u^3$	10
Kuhlman (1958)	$Q_t = C_2\ (1 - R_u{}^3)\ (\rho/g)\ u^3$	11
Radok (1977)	$Q_t = A\ e^{tu}$	12
Dong *et al.* (2003)	$Q_t = C_3\ (1 - R_u)^2\ (\rho/g)\ u^3$	13

Note: Q_t is the total mass flux (in kg m^{-1} s^{-1}); C_{1-3} is a constant (dimensionless); ρ is the air density (in kg m^{-3}); g acceleration due to gravity (in m s^{-2}); u is the wind velocity (in m s^{-1}); R_u is the u_t/u ratio of threshold wind velocity to wind velocity (dimensionless); A is an empirical constant (in kg m^{-1} s^{-1}); t is an empirical constant (in s m^{-1}).

speed for one-minute intervals. The threshold wind speed is equal to the wind speed where the saltiphone counts are just zero and increase from thereon.

The performance of the four transport models was tested for the storm events of the rainy season in 2003. The equations of Table I were fitted to the median values of total mass flux data using the wind speeds measured at 3·25 m height. First, a curve was fitted for the median of the total mass flux that was observed in the entire event. Second, the transport models were fitted to the measured total mass flux per minute for each minute within an event. These one-minute total mass fluxes were determined by multiplying the total mass flux (Q_t) with the fraction of saltation transport for each minute. This fraction was taken as the number of hits that was registered by the saltiphone for each minute divided by the total number of hits registered during the event. Again the median value of total mass flux was used for the one-minute curve fitting. The reason for using the median value of total mass flux was the high degree of spatial variability that is usually observed in sediment transport on Sahelian sandy soils (e.g. Sterk and Stein, 1997; Visser *et al.*, 2004). In this study, it was intended to develop a model that is able to predict average sediment transport conditions in the field, and not the maximum possible amount. Therefore it was believed that fitting the sediment transport equations to the median value of total mass fluxes would give a reasonable estimate of what can be expected under certain wind and surface conditions.

Modelling sediment transport around a shrub

The change in wind speed was modelled downwind of two shrubs: a *Hyphaene thebaica* of 0·6 m height and a *Commiphora africana* of 1·9 m height (Figure 3). The optical porosity (θ) of *H. thebaica* was 18%, and 79% for *C. africana*. The values of θ were determined by digital photogrammetry, similar to the method used by Kenney (1987). A digital photograph of part of the canopy was taken at approximately 25 cm from the canopy with a digital camera with a resolution of 2·1 Mega pixels and turned into black and white. The threshold value to turn pixels into black or white was visually determined. The percentage of white pixels in the photograph was taken as the porosity of the canopy. This value of porosity is the optical porosity, which is not the same as the volumetric porosity. Optical porosity is generally an underestimation of volumetric porosity because much of the small-scale porosity (between leaves and branches) is beyond the resolution of analysis and the vegetation element obscures transmission of light through it (Grant and Nickling, 1998).

First, the coefficients c, d, e and f (Equations 5–8) were adapted to model the factor of change in wind speed (Φ) along the centre line of the reduction area behind a shrub. This was done by fitting Equation 4 to data that were obtained from two experiments on the change of wind speed measured around the *Hyphaene thebaica* (Leenders *et al.*, 2007). These datasets were obtained at 0·40 m above the soil surface. One of the datasets was obtained with an average wind speed of 2·8 m s^{-1}, the other with an average wind speed of 4·2 m s^{-1} (at 0·40 m). The datasets comprised 436 and 450 observations of average wind speed per minute, normalized with upwind average wind speed per minute at different locations around the shrub. As such, these observation points represent the factor of change in wind speed (Φ) around a shrub. The observation points were interpolated to a grid with spacing of 0·1 m with a triangle-based linear interpolation (Leenders *et al.*, 2007). The thus fitted coefficients of c to f were tested with a dataset of changes in wind speed around the *Commiphora africana*. This dataset was obtained at 0·45 m height, with an average wind speed of 3·85 m s^{-1} at 0·45 m above the soil surface. It comprised 462 observations of average wind speed per minute, normalized with upwind average wind speed per minute at different locations around the shrub (Leenders *et al.*, 2007). This dataset was also interpolated to a grid with spacing of 0·1 m with a triangle-based linear interpolation.

Second, the developed model to simulate changes in sediment transport around a shrub was run for the events of 2002 around the *Hyphaene thebaica* only. It was validated with the total mass fluxes around the *H. thebaica* that were measured during the rainy season of 2002 (Leenders *et al.*, 2007). This comprised data from 54 observation points on changes in total mass flux at different locations around the *H. thebaica*. These observations were interpolated to a grid with

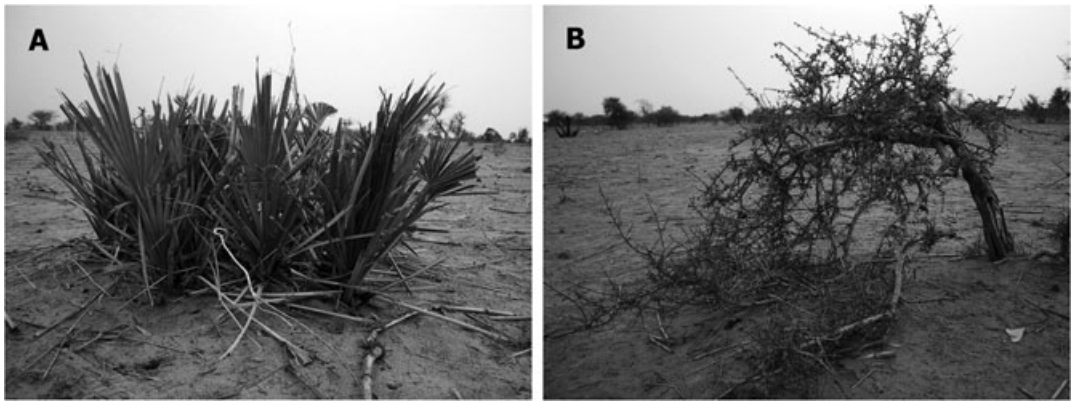

Figure 3. (A) *Hyphaene thebaica* of 0·6 m height and (B) *Commiphora africana* of 1·9 m height, both at the experimental field, Windou, north Burkina Faso.

spacing of 0·1 m with a triangle-based linear interpolation (Leenders *et al.*, 2007). For the *Commiphora africana* shrub no measurements of total mass flux were available, and hence, the model could not be validated for sediment transport around this shrub.

Results

Fit of transport equations

For the rainy season of 2003, a total of 10 wind erosion events occurred. Two events were of low intensity and lasted only a few minutes, while the record of one event was incomplete due to malfunctioning of the saltiphone. Therefore data from only seven events were used in the analysis.

The variation between the events was large (Table II). Some events lasted less than 30 minutes whereas others lasted more than an hour. The average wind direction as well as the mean wind velocity varied considerably between events (compare for example the events of 16 May and 26 June). In addition, wind velocity and wind direction differed during an event. For example, the wind direction during the event of 27 May had a standard deviation of 37°. This indicates the local character of events (Figure 4).

The observed total mass fluxes (Figure 5) were of the same order of magnitude as those observed by Sterk and Raats (1996) in the south of Niger. Measured total mass flux varied from event to event. The range in total mass flux that was observed with the 17 MWAC catchers for a single event was large. For instance, during the event of 1 July the total mass flux ranged from 0·005 to 0·033 kg m^{-1} s^{-1}, while the median value was 0·021 kg m^{-1} s^{-1}. This indicates the high spatial variability in total mass fluxes, which was also observed by Sterk and Stein (1997) and Visser *et al.* (2004). It should be noted that the total mass flux measurements do include the effects of vegetation in the study area. The entire region is covered with scattered vegetation of trees and shrubs, and most of the sandy soils are also used for pearl millet production. Hence, open areas without vegetation do not exist and our measured total mass fluxes were assumed to represent the range of total mass fluxes for individual storms that can be expected in the Sahelian environment of the study area.

The median values of the 17 measured total mass fluxes were used to fit the four transport equations (Table I) to the average wind speed for the entire event duration. The equation of Radok (1977) showed the best fit with an R^2 of 0·68. The equation of Dong *et al.* (2003) performed second best and gave an R^2 of 0·62. The poorest fit ($R^2 = 0·47$) was obtained with the equation of O'Brien and Rindlaub (1936). The number of observations in this first analysis was limited to seven events, but the results were substantiated by the analysis on total mass fluxes for each minute within an event (Table III). The equation of Radok (1977) had again the highest R^2 for six of the seven events. It showed a good fit for the events of 4 June ($R^2 = 0·78$) and 26 June ($R^2 = 0·82$), and reasonable fits ($R^2 = 0·43$–$0·51$) for the other five events. With the equation of Dong *et al.* (2003) a good fit was obtained for the event of 4 June ($R^2 = 0·73$), but a poor fit was obtained for the event of 8 July ($R^2 = 0·17$). Because the equation of Radok performed best for most of the events, Radoks' equation was selected for further model development.

Although the equation of Radok (1977) best fitted the data of both the entire event duration as well as the one-minute data during an event, the empirical constants A and t differed per fit (Table IV). The constants, however, seemed to be related: when A was plotted against t, a fit of an exponential curve through the data explained the variance in A for 82%. Therefore, the sediment transport data of each minute within an event were also fitted to the equation of Radok (1977) by fixing the empirical constant t to 0·70 for each event (Table IV). The value of 0·70 was chosen because it was the average of the fitted values of t, for all events using both saltiphones. Although slightly lower, the resulting R^2-values were comparable to those obtained through an optimal fit of both A and t. The only exception was the event of 27 May, which resulted in a low R^2 value (0·12) due to the large difference between the fixed t-value (0·70) and the initially fitted t-value (0·35). A constant value for A, that would represent the soil conditions during the event, keeping t fixed to 0·70, was not obtained. This was attributed to the variability of soil characteristics (e.g. soil moisture, crusting and crop growth) during the early rainy season.

Table II. Wind characteristics of seven wind erosion events at the experimental field at Windou, north Burkina Faso, May–July 2003

Date	Duration (minutes)	Wind velocity at 3·25 m (m s^{-1})		Wind direction at 2·25 m (deg)	
		Mean	Standard deviation	Mean	Standard deviation
16 May 2003	91	9·2	1·0	153	9
27 May 2003	31	10·1	2·0	136	37
4 June 2003	31	9·2	1·9	79	6
19 June 2003	51	11·6	1·2	104	11
26 June 2003	18	12·7	1·6	59	6
1 July 2003	19	12·9	1·5	125	7
8 July 2003	25	11·2	1·1	132	6

Modelling sediment transport around a single vegetation element

Figure 6 shows the interpolated wind speed data at the centre line downwind of the *Hyphaene thebaica* and *Commiphora africana* that were obtained from the dataset of wind speed measurements around shrubs (Leenders *et al.*, 2007). Figure 6 shows the effect of porosity and downwind distance from the shrub on the reduction of wind speed. The two experiments around the *H. thebaica* showed similar results. The *H. thebaica* influenced wind speed at 0·40 m above the soil surface to a distance of about 7·5 times its height (Figure 6A). This was similar for the *C. africana* (Figure 6B). For a windbreak with a porosity similar to that of the two shrubs this distance was estimated at 35 times the windbreak height (Hagen, 1996). In addition, Cleugh (1998) measured zones of reduced wind speed up till 30–35 times the windbreak height for porosities varying between 10% and 73%. Thus the leeward distance over which these particular shrubs affect wind speed is about four times less than the leeward distance over which a windbreak affects wind speed. This difference in distance was attributed to the different ratio of height over width for single vegetation elements compared with windbreaks. For shrub-type vegetation elements, the width and height of the element are of the same order of magnitude. As a result, the effects of wind that is forced around the shrub are important (Wolfe and Nickling, 1993), and affect the leeward distance over which a shrub exerts influence along the centreline. For windbreaks, the width of the windbreak is much larger than the height. Therefore, wind speed in the lee of a windbreak along the centreline is not much affected by wind that is flowing along the sides of a windbreak. As such, the distance over

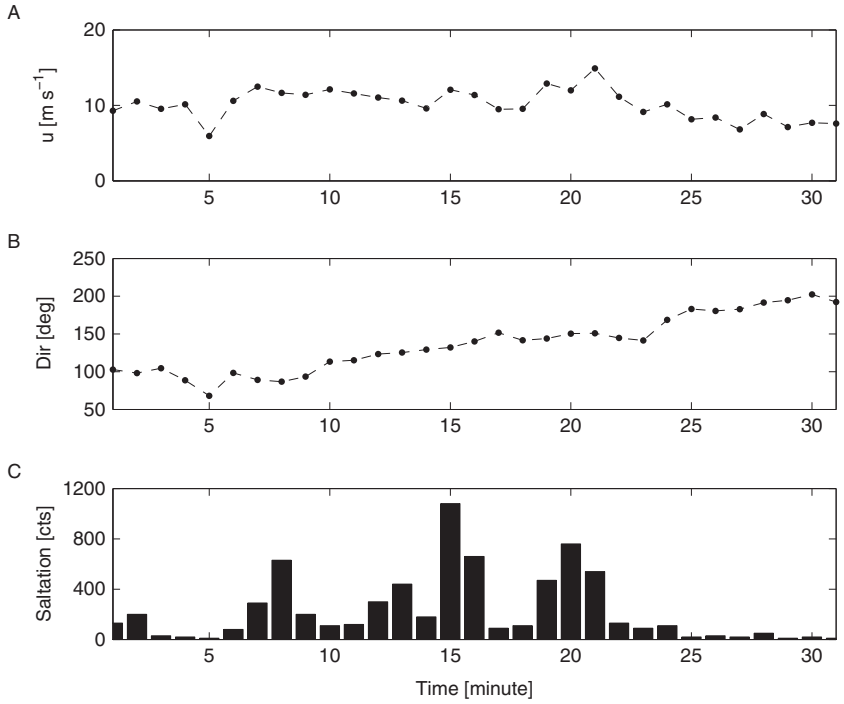

Figure 4. Thirty minutes of the storm event at Windou, north Burkina Faso, on 27 May 2003. (A) Wind velocity; (B) wind direction; (C) saltation transport.

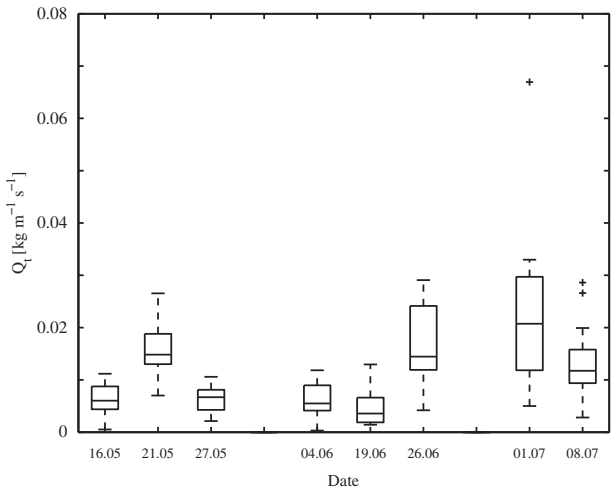

Figure 5. Measured total mass flux (Q_t) of seven wind erosion events from May to July 2003, at the experimental field, at Windou, north Burkina Faso. The lower and upper lines of the box are the 25th and 75th percentile of the sample, the distance between the top and bottom of the box is the inter-quartile range. The line in the middle of the box is the sample median. If the median is not centred in the box, as was the case on 26 June, the sample is skewed. The lines extending above and below the box show the extent of the rest of the sample. Outliers are indicated by a plus sign at the top of the plot.

which a windbreak affects wind speed in its lee is larger than for a shrub.

The reduction in wind speed behind the *Commiphora africana* was less than behind the *Hyphaene thebaica* (Figure 6). This was attributed to the higher (optical) porosity of the *C. africana* (79%) compared to the *H. thebaica* (18%). The interpolated wind speed data at the centreline downwind of the *H. thebaica* as shown in Figure 6A were used to fit and modify the coefficients *c*, *d*, *e* and *f* of Equation 4 for a shrub-type vegetation element. This resulted in:

$$c = 13(0.008 - 0.17\theta + 0.17\theta^{1.05}) \quad (14)$$

$$d = 1.05\exp(-0.5\,\theta^{0.2}) \quad (15)$$

$$e = 2.5(1 - 0.5\,\theta) \quad (16)$$

$$f = 5 - \theta \quad (17)$$

where θ is the porosity of the vegetation element.

The validity of the coefficients *c*–*f*, as expressed in Equations 14–17, was tested with the dataset along the centreline behind the *Commiphora africana* (Figure 6B). Using the coefficients *c*–*f* calculated from Equations 14–17 in Equation 4, an average reduction in wind speed of 23% along the centre line downwind of the *C. Africana* was calculated. In the dataset of Leenders *et al.* (2007) a reduction in wind speed of 27% was measured behind the *C. africana*. So, the model slightly underestimated the reduction in wind speed.

With the calculated values for reduction in wind speed on the centreline downwind of a shrub an adapted wind speed was calculated, which was used in the Radok (1977) equation to calculate the change in total mass flux. A typical pattern of the factor of reduction in wind speed (Φ) and total mass flux (ψ) in the lee of the *Hyphaene thebaica* shrub is shown in Figure 7. In the immediate lee of the shrub, sediment transport is limited, and it gradually recovers to an undisturbed total mass flux ($\psi = 1$) at a distance of 7·5 times the height of the vegetation element.

The sediment transport around the *Hyphaene thebaica* shrub was modelled for all wind erosion events of 2002. The *t*-value in the Radok (1977) equation was set at 0·7, and the *A*-values were derived from fitting the Radok equation to the measured total mass fluxes in the field (Table V). Overall, an average reduction in total mass flux of 58% was modelled along the centreline behind the *H. thebaica*. The reduction in measured total mass flux along the centreline behind this element was 53%. Hence, the modelled reduction in total mass flux along the centreline slightly overestimated the observed reduction.

Table III. Fits of total mass flux per minute to four transport equations for seven storm events at the experimental field at Windou, north Burkina Faso

Date	*n* (minutes)	R^2 O'Brien and Rindlaub, 1936 (Equation 10)	R^2 Kuhlman, 1958 (Equation 11)	R^2 Radok, 1977 (Equation 12)	R^2 Dong *et al.*, 2003 (Equation 13)
16 May 2003	91	0·27	0·30	0·51	0·55
27 May 2003	31	0·40	0·43	0·48	0·37
4 June 2003	31	0·53	0·57	0·78	0·73
19 June 2003	51	0·19	0·20	0·44	0·37
26 June 2003	18	0·28	0·31	0·82	0·36
1 July 2003	19	0·30	0·30	0·49	0·31
8 July 2003	25	0·16	0·16	0·43	0·17

Table IV. Empirical constants *A* and *t* of the Radok (1977) equation, for each storm event in 2003, together with goodness-of-fit for the optimal fit and in case of $t = 0{\cdot}7$ s m^{-1}

Date	Optimal fit *A* and *t*			Best fit *A*, $t = 0{\cdot}7$ (s m^{-1})	
	A	*t*	R^2	*A*	R^2
	(kg m^{-1} s^{-1})	(s m^{-1})		(kg m^{-1} s^{-1})	
16 May 2003	9·65E–09	0·92	0·51	8·54E–08	0·48
27 May 2003	5·51E–06	0·35	0·48	2·86E–08	0·12
4 June 2003	2·03E–07	0·67	0·78	1·09E–07	0·78
19 June 2003	1·04E–08	0·74	0·44	1·36E–08	0·42
26 June 2003	2·09E–07	0·62	0·82	4·77E–08	0·81
1 July 2003	1·51E–06	0·50	0·49	2·27E–07	0·47
8 July 2003	3·40E–07	0·64	0·43	3·83E–07	0·39

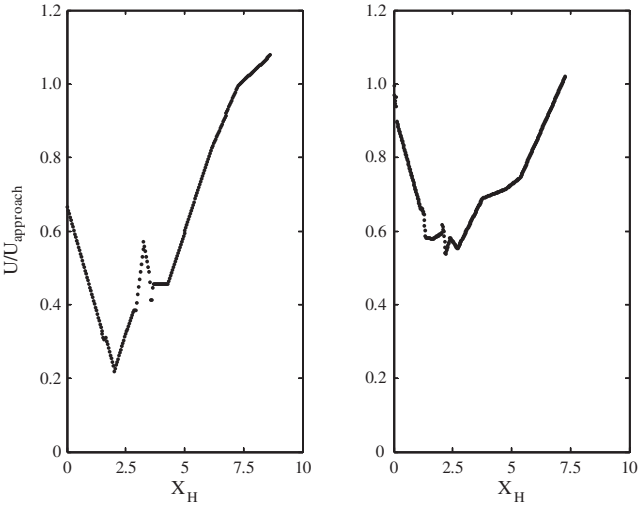

Figure 6. Wind speed reduction in the lee of a shrub, in the direction of the wind. The wind speed at any distance (*U*), is normalized by the approach wind speed ($U_{approach}$) and plotted against the downwind distance from the shrub in terms of shrub height units (x_H). Left: *Hyphaene thebaica* of 0·6 m height, wind speed was measured at 0·40 m. Right: *Commiphora africana* of 1·9 m height, wind speed was measured at 0·45 m.

Also for the entire area of reduction downwind of the *H. thebaica*, the model overestimated the total mass flux. The model predicted a reduction of 57% in total mass flux in the reduction zone, whereas a reduction of 49% was derived from measurements.

Because of the variability in wind directions during an event, the total reduction area during an event was 1·8–3·6 times the area of one reduction ellipse (Table V). As a consequence, the average factor of reduction in total mass flux downwind of the shrub increased. Figure 8 shows an example of the model for the event of 7 June 2002. The average wind direction during this event was 180°, it varied from 134° to 224°. As a result the total reduction area was 3·6 times larger than the area of one reduction ellipse.

For the zone of increase in wind speed, the effect of wind direction was not as strong as in the area of reduction in sediment transport. The area of increase in sediment transport at the sides of the vegetation element was 1·2–1·8 times larger because of a varying wind direction. The effect was smaller in this area compared to the zone of reduction, because the zone

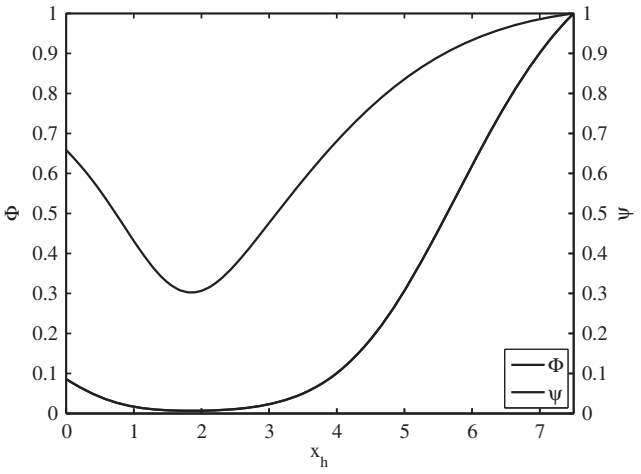

Figure 7. Typical pattern of modelled change in wind speed (Φ) and total mass flux (ψ) as a function of distance from the shrub in terms of shrub height (x_H) in the lee of a *Hyphaene thebaica* of 0·6 m height.

Table V. Results of sediment transport modelling around a *Hyphaene thebaica* of 0·6 m height for 10 events during the rainy season of 2002 at Windou, north Burkina Faso

Date	A(kg m^{-1} s^{-1})	Wind direction (deg)			Reduction in Q_t		Increase in Q_t	
		Minimum	Maximum	Range	F	ψ	F	ψ
3 June 2002	9·53E–08	117	141	24	1·8	0·69	1·3	1·21
4 June 2002	5·47E–08	83	121	38	2·3	0·67	1·3	1·56
7 June 2002	6·71E–07	134	224	90	3·6	0·80	1·8	1·28
11 June 2002	2·23E–07	130	155	25	1·9	0·62	1·3	1·38
14 June 2002	1·90E–08	94	140	46	2·6	0·79	1·4	1·17
24 June 2002	6·67E–08	77	107	30	1·9	0·65	1·2	1·34
29 June 2002	5·98E–08	79	143	64	3·2	0·76	1·5	1·47
13 July 2002	3·27E–07	16	45	29	2·1	0·61	1·4	1·60

Note: A is the constant in the Radok (1977) equation; Q_t is the total mass flux; F is the factor at which the area of reduction or increase in total mass flux is enlarged. (The area of reduction with a uniform wind direction is 4·95 m^2, for the area of increase this is 1·54 m^2); ψ is the sediment transport change factor.

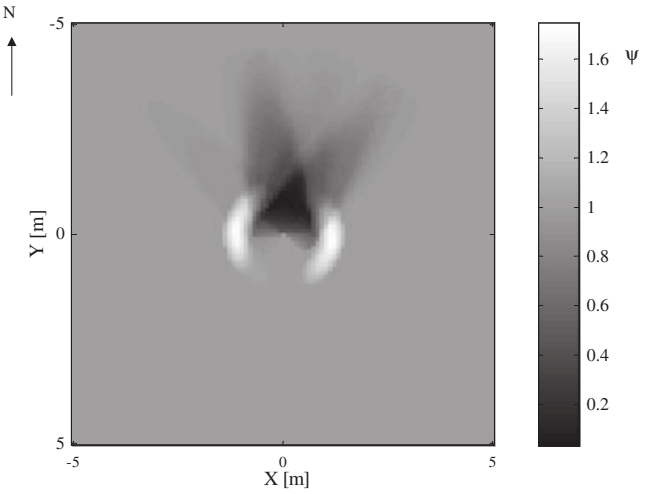

Figure 8. Simulated average factor of change in total mass flux (ψ) around a *Hyphaene thebaica* of 0·6 m height for the storm event of 7 June 2002 at Windou, north Burkina Faso.

of increased total mass flux was positioned closer to the vegetation element than the zone of reduction of total mass flux (Figure 8). The sediment transport factor (ψ) in the zone of increase of total mass flux was estimated by the model as 1·38, while the measured factor was 1·16 (Leenders *et al.*, 2007). This overestimation was assumed acceptable because the interpolation of measured total mass flux was based on 54 points only, while wind speed was based on 440 points. As such, the factor of change in wind speed, as derived from field measurements, was considered more reliable than the factor of change in total mass flux derived from field measurements. Therefore, it was decided not to adapt the model for the sediment transport factor in the zone of increased sediment transport to the sides of the shrub.

Discussion and Conclusion

The measured sediment transport was predicted best with a simple empirical equation of Radok (1977). It expresses the total mass flux being exponential to the wind velocity and two empirical constants. One of the empirical constants t is the 'growth' factor of sediment transport and could be fixed at 0·7 s m^{-1} for each storm. The other empirical constant (A) can be interpreted as the erodibility of the soil. But the variability of events in this study was so diverse that this 'erodibility' parameter could not be fixed. It showed an increasing trend during the growing season. The analysis of this study raises the question as to whether a general transport model exists, knowing that field conditions are variable, both in space and time. It was concluded that in order to predict sediment transport adequately, modelling results should always be supported and substantiated by actual measurements of sediment transport due to the inaccurate assessment of the soil erodibility factor (A).

A model was developed to simulate wind speed and sediment transport around a single shrub-type vegetation element. In this model, porosity, height and width of the vegetation element determine the extent of the wake zone. Porosity mainly determines the position of minimum wind speed and the rate of recovery of wind speed. A curve describing wind speed changes in the lee of a shrub with a porosity of only 18% was derived using actual measurements of wind speed reductions. This curve, which is a function of the shrub's porosity, height and width, was subsequently tested for a shrub with a porosity of 79% and slightly underestimated the measured reduction (23% reduction modelled versus 27% reduction measured). The estimation of wind speed along the centreline in the lee of the shrub up to 7·5 times the element height was similar to actual measurements. But, it should be mentioned that very dense obstacles can induce an area of re-circulating eddies in the immediate lee, with increased turbulence (Cleugh, 1998). For such obstacles the wind speed changes show a lower minimum wind speed, because the rate of wind speed recovery is faster near the lee of the obstacle and slower thereafter. Low porosity obstacles are assumed to be less effective in reducing wind velocity than medium porosity obstacles (Wang and Takle, 1996). Cornelis and Gabriels (2005) concluded that a porosity of 20–35% is optimal for wind barriers in terms of wind-velocity reduction.

Ruck and Schmitt (1986) who used Laser-Doppler-Anemometry in a wind tunnel, also showed that porosity, height and width of an obstacle determine the extent of a wake zone. They also found that airflow around a vegetation element with a trunk differed from that without, due to the flow underneath the canopy. This difference was noticed immediately downwind of the obstacle as well as further downwind. Leenders *et al.* (2007) illustrated this difference in morphology among vegetation elements with respect to the airflow pattern from experimental results in a farmer's field.

Gross (1987) developed a numerical model for the airflow around individual trees, both with and without a trunk. His results corresponded qualitatively well with the wind tunnel

measurements of Ruck and Schmitt (1986). The model of Gross (1987) is physically based. It uses the Navier–Stokes equations, the continuity equation and the first law of thermodynamics. Application of the model is complicated and requires measurement or estimation of many different input variables. The model presented here is empirically based and is a relatively simple model and therefore easy to apply by researchers, extension workers and others who aim to develop wind erosion control strategies that use scattered vegetation. It only simulates wind flow and sediment transport around shrubs. Currently it can not be used to simulate sediment transport near trees.

For the shrub tested in this study, a reduction of 57% in total mass flux was simulated in its lee. To the sides an increase of 38% in total mass flux was simulated. The result of these opposite effects, i.e. an increase in sediment transport on the sides of the shrub and a decrease in its lee zone, creates small hills under the canopy of the shrub. Usually shrubs are located on micro-dunes due to trapping of sediment in the canopy (Sterk *et al.*, 2004). This process of deflation in areas between vegetation and the subsequent trapping of saltation material by canopies was called 'pedestalling' by Okin *et al.* (2006). As wind directions are variable during Sahelian storms, the zones of increase in sediment transport are not visible as distinct channels, but merely cause an overall lowering of the soil profile on the windward sides of the shrubs. Only after a strong storm with a constant wind direction the particular profile as given in Figure 1 could become visible. However, due to the normal variations in wind direction during a storm the erosion-sedimentation pattern is usually less clear.

Because the area of the zone of reduction in total mass flux was larger than the area of the zones of increase in total mass flux, the model simulated a net reduction in total mass flux around the shrub, which is in agreement with field measurements (Leenders *et al.*, 2007). In addition, during a storm event with variable wind directions, the area over which a shrub affects total mass flux increased. These findings suggest that shrubs, being scattered in a farmer's field could be used to reduce and control sediment transport, and thus wind erosion in a field. But, in order to develop a control strategy that uses shrubs or scattered woody vegetation to control sediment transport, it is necessary to understand the effects of scattered vegetation on a larger scale than a single vegetation element, i.e. the scale of a field or several fields. These effects comprise the arrangement of vegetation elements together with the distribution in type, height, width and porosity of vegetation elements, the interaction between vegetation elements and their effects to extract momentum from the air at a larger scale (Gross, 1987; Wolfe and Nickling, 1993; Musick *et al.*, 1996). The model presented in this paper is not yet adequate to describe these conditions and therefore will be further developed to include the effects of trees on wind speed and sediment transport. If scaled up effectively, the model could be used to determine the effect of different vegetation patterns with different vegetation characteristics. The results could subsequently be used to develop wind erosion control strategies by using scattered vegetation.

Acknowledgements—The authors are grateful to NWO-WOTRO, The Netherlands Organization for Scientific Research in the Tropics, for financing and supporting this research.

References

Alfaro SC, Rajot JL, Nickling W. 2004. Estimation of PM20 emissions by wind erosion: main sources of uncertainties. *Geomorphology* **59**: 63–74.

Ash JE, Wasson RJ. 1983. Vegetation and sand mobility in the Australian desert dunefield. *Zeitschrift fur Geomorphology Supplementband* **45**: 7–25.

Bagnold RA. 1941. *The Physics of Blown Sand and Desert Dunes*. Methuen: London; 265 pp.

Bielders CL, Alvey S, Cronyn N. 2001. Wind erosion: the perspective of grass-roots communities in the Sahel. *Land Degradation & Development* **12**: 57–70.

Camp DW, Turner RE, Gilchris LP. 1970. Response tests of cup, vane and propeller wind sensors. *Journal of Geophysical Research* **75**: 5265–5270.

Chepil WS. 1956. Influence of moisture on erodibility of soil by wind. *Soil Science Society of America Journal* **20**: 288–292.

Cleugh HA. 1998. Effects of windbreaks on airflow, microclimates and crop yields. *Agroforestry Systems* **41**: 55–84.

Cornelis WM, Gabriels D. 2005. Optimal windbreak design for wind erosion control. *Journal of Arid Environments* **61**: 315–332.

Cornelis WM, Oltenfreiter G, Gabriels D, Hartman R. 2004. Splash-saltation of sand due to wind-driven rain: horizontal flux and sediment transport rate. *Soil Science Society of America Journal* **68**: 41–46.

Dong Z, Liu X, Wang H, Wang X. 2003. Aeolian sand transport: a wind tunnel model. *Sedimentary Geology* **161**: 71–83.

Fryrear DW. 1985. Soil cover and wind erosion. *Transactions of the ASAE* **28**: 781–784.

Fryrear DW, Krammes CA, Williamson DL, Zobeck TM. 1994 Computing the wind erodible fraction of soils. *Journal of Soil and Water Conservation* **49**: 183–188.

Goossens D. 2004. Effect of soil crusting on the emission and transport of wind-eroded sediment: field measurements on loamy sandy soil. *Geomorphology* **58**: 145–160.

Goossens D, Offer Z, London G. 2000. Wind tunnel and field calibration of five aeolian sand traps. *Geomorphology* **35**: 233–252.

Grant PF, Nickling WG. 1998. Direct field measurement of wind drag on vegetation for application to windbreak design and modelling. *Land Degradation and Development* **9**: 57–66.

Greely R, Iversen JD. 1985. *Wind as a Geological Process*. Cambridge University Press: Cambridge.

Gross G. 1987. A numerical study of the air flow within and around a single tree. *Boundary-Layer Meteorology* **40**: 311–327.

Hagen LJ. 1996. *WEPS: Wind Erosion Prediction System*, Technical Documentation. Wind Erosion Research Unit: Manhattan, KS.

Iversen JD, Rasmussen KR. 1999. The effect of wind speed and bed slope on sand transport. *Sedimentology* **46**: 723–731.

Kenney WA. 1987. A method for estimating windbreak porosity using digitized photographic silhouettes. *Agricultural and Forest Meteorology* **39**: 91–94.

Kuhlman H. 1958. Quantitative measurements of aeolian sand transport. *Geografisk Tidsskrift* **57**: 51–74.

Leenders JK, Van Boxel JH, Sterk G. 2005a. Wind forces and related saltation transport. *Geomorphology* **71**: 357–372.

Leenders JK, Van Boxel JH, Sterk G. 2007. The effect of single vegetation elements on wind speed and sediment transport in the Sahelian zone of Burkina Faso. *Earth Surface Processes and Landforms* **32**: 1454–1474.

Leenders JK, Visser SM, Stroosnijder L. 2005b. Farmers' perceptions of the role of scattered vegetation in wind erosion control in Burkina Faso. *Land Degradation & Development* **16**: 327–337.

Marshall JK. 1971. Drag measurements in roughness arrays of varying density and distribution. *Agricultural Meteorology* **8**: 269–292.

McKenna Neuman C. 1998. Particle transport and adjustments of the boundary layer over rough surfaces with an unrestricted, upwind supply of sediment. *Geomorphology* **25**: 1–17.

Michels K, Sivakumar MVK, Allison BE. 1995. Wind erosion control using crop residue I. Effects on soil flux and soil properties. *Field Crops Research* **40**: 101–110.

Mohammed AE, Stigter CJ, Adam HS. 1995. Moving sand and its consequences on and near a severely desertified environment and a protective shelterbelt. *Arid Soil Research and Rehabilitation* **9**: 423–435.

Musick HB, Gillette DA. 1990. Field evaluation of relationships between a vegetation structural parameter and sheltering against wind erosion. *Land Degradation & Rehabilitation* **2**: 77–85.

Musick HB, Trujillo SM, Truman CR. 1996. Wind-tunnel modelling of the influence of vegetation structure on saltation threshold. *Earth Surface Processes and Landforms* **21**: 589–605.

Namikas SL, Bauer BO, Sherman DJ. 2003. Influence of averaging interval on shear velocity estimates for aeolian transport modeling. *Geomorphology* **53**: 235–246.

Namikas SL, Sherman DJ. 1995. A review of the effects of surface moisture content on aeolian sand transport. In *Desert Aeolian Processes*, Tchakerian VP (ed.). Chapman and Hall: London; 269–293.

O'Brien MP, Rindlaub BD. 1936. The transportation of sand by wind. *Civil Engineering* **6**: 325–327.

Okin GS. 2008. A new model for wind erosion in the presence of vegetation. *Journal of Geophysical Research, Earth Surface* **113**: F02S10.

Okin GS, Gillette DA, Herrick JE. 2006. Multi-scale controls on and consequences of aeolian processes in landscape change in arid and semi-arid environments. *Journal of Arid Environments* **65**: 253–257.

Radok U. 1977. Snow drift. *Journal of Glaciology* **19**: 123–139.

Raupach MR, Thom AS, Edwards I. 1980. A wind-tunnel study of turbulent flow close to regularly arrayed rough surfaces. *Boundary-Layer Meteorology* **18**: 373–397.

Raupach MR, Woods N, Dorr G, Leys JF, Cluegh HA. 2001. The entrapment of particles by windbreaks. *Atmospheric Environment* **35**: 3373–3383.

Rice MA, McEwan IK. 2001. Crust strength: a wind tunnel study of the effect of impact by saltating particles on cohesive soil surfaces. *Earth Surface Processes and Landforms* **26**: 721–723.

Rinaudo T. 1996. Tailoring wind erosion control methods to farmers' specific needs. In *Proceedings of the International Symposium on 'Wind Erosion in West Africa: The Problem and its Control'*, Hohenheim, Germany, 5–7 December 1994, Buerkert B, *et al*. (eds). Margraf Verlag: Weikersheim.

Ruck VB, Schmitt F. 1986. Das Strömungsfeld der Einzelbaumuströmung. Abschätzung von Depositionswahrscheinlichkeiten für Feinsttröpfchen. *Forstwissenschaftliches Centralblatt* **105**: 178–196.

Schlichting H. 1936. Experimental untersuchugungen zum rauhigkeitsproblem. *Ingenieur Archiv* **7**: 1–34.

Schönfeldt HJ, Von Löwis S. 2003. Turbulence-driven saltation in the atmospheric surface layer. *Meteorologische Zeitschrift* **12**: 257–268.

Shao Y. 2000. *Physics and Modelling of Wind Erosion*, Atmospheric and Oceanographic Sciences Library, Vol. **23**. Kluwer Academic Publishers: Dordrecht.

Sherman DJ, Jackson DWT, Namikas SL, Wang J. 1998. Wind-blown sand on beaches: an evaluation of models. *Geomorphology* **22**: 113–133.

Spaan WP, Van den Abeele GD. 1991. Wind borne particle measurements with acoustic sensors. *Soil Technology* **4**: 51–63.

Sterk G. 1993. *Sahelian Wind Erosion Research Project, Report III. Description and Calibration of Sediment Samplers*. Department of Irrigation and Soil and Water Conservation, Wageningen University: Wageningen.

Sterk G. 2003. Causes, consequences and control of wind erosion in Sahelian Africa: a review. *Land Degradation & Development* **14**: 95–108.

Sterk G, Haigis J. 1998. Farmers' knowledge of wind erosion processes and control methods in Niger. *Land Degradation & Development* **9**: 107–114.

Sterk G, Hermann L, Bationo A. 1996. Wind-blown nutrient transport and soil productivity changes in southwest Niger. *Land Degradation & Development* **7**: 325–335.

Sterk G, Jacobs AFG, Van Boxel JH. 1998. The effect of turbulent flow structures on saltation transport in the atmospheric boundary layer. *Earth Surface Processes and Landforms* **23**: 877–887.

Sterk G, Lopez MV, Arrue JL. 1999. Saltation transport on a silt loam soil in northeast Spain. *Land Degradation & Development* **10**: 545–554.

Sterk G, Raats PAC. 1996. Comparison of models describing the vertical distribution of wind-eroded sediment. *Soil Science Society of America Journal* **60**: 1914–1919.

Sterk G, Stein A. 1997. Mapping wind-blown mass transport by modelling variability in space and time. *Soil Science Society of America Journal* **61**: 232–239.

Sterk G, Stein A, Stroosnijder L. 2004. Wind effects on spatial variability in pearl millet yields in the Sahel. *Soil & Tillage Research* **76**: 25–37.

Stockton PH, Gillette DA. 1990. Field measurements of the sheltering effect of vegetation on erodible land surfaces. *Land Degradation & Rehabilitation* **2**: 77–85.

Taylor-Powell E. 1991. *Integrated Management of Agricultural Watersheds: Land Tenure and Indigenous Knowledge of Soil and Crop Management. T. S. B. 91-04*. Texas A&M University: College Station, TX.

Van de Ven TAM, Fryrear DW, Spaan WP. 1989. Vegetation characteristics and soil loss by wind. *Journal of Soil and Water Conservation* **44**: 347–349.

Visser SM, Sterk G, Snepvangers JJJC. 2004. Spatial variation in wind-blown sediment transport in geomorphic units in northern Burkina Faso using geostatistical mapping. *Geoderma* **120**: 95–107.

Wang H, Takle ES. 1996. Momentum budget and shelter mechanism of boundary-layer flow near a shelterbelt. *Boundary-Layer Meteorology* **82**: 417–435.

Wolfe SA, Nickling WG. 1993. The protective role of sparse vegetation in wind erosion. *Progress in Physical Geography* **17**: 50–68.

Wolfe SA, Nickling WG. 1996. Shear stress partitioning in sparsely vegetated desert canopies. *Earth Surface Processes and Landforms* **21**: 607–619.

Zingg AW. 1953. Wind-tunnel studies of the movement of sedimentary material. In *Proceedings of the 5th Hydraulic Conference*, Iowa City. Institute of Hydraulics, University of Iowa Studies: Iowa City, IA; 111–135.